Optical Engineering

SPIEDigitalLibrary.org/oe

Effectiveness of multisite diversity schemes to support optical systems in scientific missions

Lorenzo Luini
Roberto Nebuloni
Carlo Capsoni

SPIE

Effectiveness of multisite diversity schemes to support optical systems in scientific missions

Lorenzo Luini,[a] Roberto Nebuloni,[b,*] and Carlo Capsoni[a,b]
[a]Politecnico di Milano, Dipartimento di Elettronica, Informazione e Bioingegneria (DEIB), Piazza Leonardo da Vinci 32, Milano 20133, Italy
[b]Consiglio Nazionale delle Ricerche, Istituto di Elettronica e di Ingegneria dell'Informazione e delle Telecomunicazioni, Via Ponzio 34/5, Milano 20133, Italy

Abstract. This contribution investigates the effectiveness of optical communication links in enabling high-speed data transfer from deep-space (DS) probes directly to Earth ground stations. In particular, the propagation impairments induced by clouds are estimated by exploiting long-term radiosonde observation data collected in some European sites. The impact of different cloud types on optical links operating at 1.55 μm is first quantified in terms of total path attenuation, and afterward, the implementation of multisite diversity schemes is discussed to counteract the extremely high attenuation levels caused by clouds. Results show that a three-site diversity system with target availability of 90% allows reduction of the link margin to counteract cloud attenuation from at least 40 dB to ~6 dB, which makes optical communications a viable option also for DS missions. [DOI: 10.1117/1.OE.53.2.026104]

Keywords: atmospheric propagation; atmospheric scattering; free-space optics.

Paper 131827 received Dec. 3, 2013; revised manuscript received Jan. 20, 2014; accepted for publication Jan. 23, 2014; published online Feb. 18, 2014.

1 Introduction

A key driver to the use of optical communication links (OCLs) is the availability of very large bandwidths to support high-data-rate transmission.[1,2] In space applications, optical bands are an attractive alternative to radio frequencies for transferring the increasingly high amounts of data collected by the sensors onboard Earth observation satellites or interplanetary probes. Possible mission scenarios for space-to-ground optical communications include low Earth orbit (LEO), high elliptical orbit (HEO), or geostationary Earth orbit (GEO) satellites, lunar, Lagrangian points, and deep-space (DS), i.e., links from vehicles beyond the Earth-sun distance.[3] Optical transmission experiments carried out so far involve terminals onboard platforms orbiting the Earth. An up-to-date review is given in Ref. 4. The National Aeronautics and Space Administration (NASA) lunar mission Lunar Atmosphere and Dust Environment Explorer (LADEE), launched in September 2013, features a laser demonstrator for broadband communications with Earth stations.[5]

Link budgets of optical systems for space applications must include a link margin to cope with the effects of the Earth's atmosphere. The propagation of optical waves through the atmosphere is impaired by gases, atmospheric particles (fog, clouds, rain, etc.), and clear-air turbulence. Optical windows free from molecular absorption include the visible region and the wavelengths traditionally used in fiber optics, i.e., 0.85 and 1.55 μm. The 1.064-μm wavelength, which exhibits a minimum in the gaseous absorption, is attractive as well for DS systems, due to heavy constraints on the link budget that limit the margin available to deal with atmospheric losses. Clear-air impairments include scintillations and angle-of-arrival fluctuations.[3,6] However, arrays of ground telescopes spaced by a distance larger than the Fried parameter (i.e., the spatial scale of coherence of an optical beam) or large single receiver apertures substantially reduce the effects of the atmospheric turbulence in the DS scenarios.[7]

This contribution investigates the impact of clouds on download laser links in a scientific mission scenario, where a 1.55-μm-optical terminal is onboard a spacecraft orbiting Mars and the other one is located on the Earth's surface. First, a model of the attenuation induced on laser beams by different types of clouds is described. Afterward, a database of radiosonde observations (RAOBS), available at some sites in Europe, is processed first to identify and classify clouds and then to statistically estimate the optical attenuation due to clouds in a typical year. Finally, this work addresses the advantage originating from implementing advanced site diversity schemes to substantially increase link availability/data rate.

2 Modeling the Effects of Clouds on Free-Space Optics (FSO) Systems

Clouds induce extremely high levels of laser attenuation due to the high extinction efficiency of droplets and to their high concentration. Typically, the atmospheric part of the link budget is compiled assuming that an OCL can be established only in cloud-free line-of-sight conditions.[3,8] In this work, the cloud attenuation is estimated from high-resolution RAOBS data and link availability is calculated from the statistics of cloud attenuation. Although most clouds exhibit very large attenuation levels, which make any OCL unfeasible, a calculation of the statistical distribution of cloud attenuation represents an obvious improvement over the classical (and too conservative) on–off channel model approach.

*Address all correspondence to: Roberto Nebuloni, E-mail: roberto.nebuloni@ieiit.cnr.it

0091-3286/2014/$25.00 © 2014 SPIE

Different cloud types are associated with different particle size distributions (PSDs), typically modeled as a modified gamma function of the following kind:[9]

$$n(r) = gr^{\alpha} \exp(-br^{\gamma}), \tag{1}$$

where b, α, and γ are parameters regulating the shape of Eq. (1), g is proportional to the cloud liquid water content (LWC), and $n(r) \cdot \mathrm{d}r$ is the number of particles per unit volume of air with radius comprised between r and $r + \mathrm{d}r$. Since the different PSDs produce different effects on propagating waves, the first step of the procedure consists in classifying clouds into four groups, each one with its associated PSD, and thickness ΔH. To this aim, we have used the ΔH values suggested in Ref. 10 (and reported here in Table 1 for convenience) for the following types of clouds: stratus, nimbostratus, cumulus, and cumulonimbus. Table 1 also lists the gamma function parameters in Eq. (1) that define the PSD for each cloud type.[9]

In this work, ΔH is calculated by processing the Fondazione Ugo Bordoni (FUB)-European Space Agency (ESA) radiosoundings (FERAS) database. We used the sondes launched twice a day (0 and 12 UTC) in nonrainy conditions in several European sites during the period 1980 to 1987.[11] Specifically, high-resolution vertical profiles of temperature, pressure, and relative humidity are used as inputs to a cloud detection algorithm[12] to identify and characterize clouds at each height level in terms of LWC and ice water content (IWC) in $\mathrm{g/m^3}$. The TKK (Teknillinen korkeakoulu—Helsinki University of Technology) cloud detection algorithm, first proposed by Salonen and Uppala[12] with the main purpose of estimating the attenuation due to clouds in the 10- to 300-GHz frequency range, identifies clouds at height levels where the relative humidity exceeds a critical threshold U_C defined as

$$U_C = 1 - \alpha\sigma(1-\sigma)[1 + \beta(\sigma - 0.5)]. \tag{2}$$

In Eq. (2), $\alpha = 1$, $\beta = \sqrt{3}$, and σ is the ratio between the pressure at the considered height level and at the ground level. If the measured humidity is higher than the critical one at the same pressure level, the layer is assumed to be within a cloud. The estimation of LWC in $\mathrm{g/m^3}$ at each level is derived from the air temperature T (°C) in the layer and from the distance of the layer from the cloud base h_c (m), according to the following relationship:[13]

$$\mathrm{LWC} = \begin{cases} w_0(1 + cT)\left(\frac{h_c}{h_r}\right) p_W(T) & T \geq 0°\mathrm{C} \\ w_0 e^{cT}\left(\frac{h_c}{h_r}\right) p_W(T) & T < 0°\mathrm{C} \end{cases}, \tag{3}$$

where $w_0 = 0.17\ (\mathrm{g/m^3})$, $c = 0.04\ (°\mathrm{C}^{-1})$, and $h_r = 1500\ (\mathrm{m})$.

The cloud liquid and ice water fraction $p_W(T)$ is given by the expression in Eq. (4), according to which liquid and ice particles coexist when $-20°\mathrm{C} \leq T \leq 0°\mathrm{C}$, while liquid-only or ice-only clouds are present when the temperature is higher than 0°C or lower than −20°C, respectively:[13]

$$p_W(T) = \begin{cases} 1 & T > 0°\mathrm{C} \\ 1 + T/20 & -20°\mathrm{C} < T \leq 0°\mathrm{C} \\ 0 & T \leq -20°\mathrm{C} \end{cases}. \tag{4}$$

Figure 1 shows sample vertical profiles extracted from the RAOBS database (collected at Milano/Linate airport, Italy), as well as the relative humidity threshold U_C with the resulting profiles of liquid and IWCs estimated by the TKK algorithm. A cumulus cloud is identified with base and top height at 2 and 4.2 km, respectively. The TKK algorithm has proven to work properly on a statistical basis (it is currently adopted by ITU-R in recommendation P.840-5 for cloud attenuation in the 10- to 300-GHz range[14]) in the identification of clouds and in the quantification of liquid and IWCs from RAOBS.[12,15]

Under the assumption of single scattering and provided that the PSD is known, the Mie theory allows to calculate the attenuation per unit length for each height level in the

Table 1 Cloud classification and associated parameters of the gamma function particle size distribution.

Cloud type	ΔH (km)	b	α	γ
Stratus	<0.7	0.6	6	1
Nimbostratus	0.7 to 1.4	0.425	4	1
Cumulus	1.4 to 3	0.5	5 to 6	0.3 to 0.5
Cumulonimbus	>3	0.5	5 to 6	0.3 to 0.5

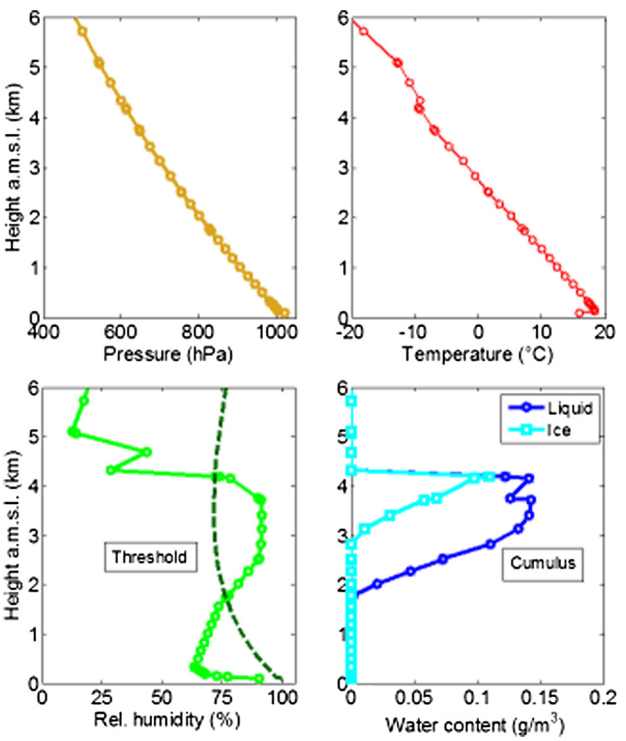

Fig. 1 Sample vertical profiles of pressure, temperature and relative humidity for a cumulus cloud from radiosonde observations collected at Milano/Linate airport. Also shown are the liquid and ice water content profiles as estimated by the TKK algorithm.

cloud, hence, the overall path attenuation, by successively integrating along the propagation path. The Mie theory holds for spherical droplets, which is the case of liquid water clouds.[16] Zenith path attenuation is therefore obtained as

$$A_V = 4.34\sum_k \Delta h_k \gamma_{I,k} = 4.34\sum_k \Delta h_k \int \sigma(r) n(r) \mathrm{d}r \ \mathrm{(dB)}, \tag{5}$$

where $\gamma_{I,k}$ is the attenuation per unit length of the k-th liquid cloud layer, Δh_k is the vertical extent of the layer, $\sigma(r)$ is Mie's extinction cross-section for a sphere of radius r, and $n(r)$ is the corresponding PSD. The PSD shape is assumed constant throughout the cloud (but dependent on cloud type according to Table 1), while the particle concentration [i.e., the parameter g in Eq. (1)] is proportional to the LWC of each layer.

As for ice clouds, we have used a simple relationship between the IWC (in $\mathrm{g/m^3}$) and the attenuation per unit length $\gamma_{I,k}$, which holds in the optical limit and represents an average over the several types of crystal shape:[17]

$$\gamma_{I,k} = 40.26(\mathrm{IWC_k})^{0.68} \ \mathrm{(dB/km)}. \tag{6}$$

As an example, based on the RAOBS data collected at Cagliari/Elmas airport (Italy), Table 2 shows, for each of the considered cloud types, the frequency of occurrence (conditioned to the presence of clouds), the average values of the liquid water column (i.e., the LWC integrated over the cloud extent), and of the associated 1.55-μm zenith attenuation: stratus clouds, by far the most common type of clouds, induce relatively low attenuation, which justifies the interest in extending the classical on-off channel approach.

3 DS Scenario

The DS scenario considered in this work is the exploration of Mars. Specifically, we have taken as reference the Mars Express mission, conceived by ESA to study the geology of Mars and investigate the possible presence of life on the planet by means of the remote sensing instruments onboard Mars Express Orbiter (e.g., MARSIS—Mars Advanced Radar for Subsurface and Ionosphere Sounding).[18] Since the beginning of 2004, the probe has been orbiting Mars along a highly elliptical trajectory of 298×10107 km^2, with a period of 6.7 h and an inclination of 86 deg (near-polar orbit). As for the possible Earth stations, we have selected the following sites located in the Mediterranean area, which appear to be suitable for this application because of their present use. They are:

1. Cebreros, Spain (lat = 40.45°N, lon = −4.37°E, altitude = 794 m a.m.s.l.) where a station of the ESA Tracking Station Network (ESTRACK) is located;
2. Cagliari, Italy (lat = 39.49°N, lon = 9.25°E, altitude = 700 m a.ms.l.) where the new Italian INAF (National Institute of Astrophysics) radio telescope is under construction;
3. Noto, Italy (lat = 36.88°N, lon = 14.99°E, altitude = 150 m a.ms.l.) where another radio telescope is operated by INAF.

Correspondingly, RAOBS data for the identification and quantification of clouds impairing the mentioned DS stations are available for:

1. Madrid/Barajas airport, 67 km from Cebreros;
2. Cagliari/Elmas airport, 31 km from the INAF radio telescope site;
3. Trapani/Birgi airport, 250 km from Noto. Although the latter distance is quite large, nevertheless, RAOBS collected at Trapani/Birgi airport can be considered to be representative of the Sicilian climate and therefore are taken as a reference for Noto as well.

In order to calculate the geometric information needed for the simulation of the FSO system, we have resorted to the SPICE Toolkit, made available by the Navigation and Ancillary Information Facility (NAIF) of the NASA.[19] SPICE was developed with the aim of assisting scientists in planning and interpreting scientific observations from space-borne instruments and supporting engineers involved in modeling, designing, and executing activities needed to conduct planetary exploration missions. In this work, SPICE has been employed to calculate the visibility windows and the elevation angle between the DS Earth stations mentioned above and Mars Express Orbiter, based on the Mars Express "mission kernels" (primary data sets consisting in navigation and other ancillary information structured for easy access by the planetary science and engineering communities) ranging from 2005 to 2012. As an example, Fig. 2 depicts the shortest (around 4 h) and longest (around 11 h) visibility windows for the three DS stations in the considered period (respectively occurred in February 2005 and in January 2008) for which the minimum elevation angle θ is set to 20 deg (see Ref. 4). Obviously, these visibility windows are respectively associated to the lowest (roughly 30 deg) and highest (~80 deg) maximum elevations of Mars as seen from the DS stations. The interruption in the visibility curves of Fig. 2(a) is associated to the probe occultation caused by the interposition of Mars between the DS stations and the probe itself.

As is clear from the discussion above, RAOBS measurements, collected between 1980 and 1987 (period P1), are not concurrent with the Mars Express mission, launched in 2003. Nevertheless, the impact of clouds on the DS stations can be statistically assessed by arbitrarily shifting the 1980 to 1987 period to synchronize it with 8 years for which Mars Expression mission data are available (2005 to 2012, period P2), such that January 1980 is associated to January 2005

Table 2 Average cloud properties obtained from radiosonde observations data collected at Cagliari/Elmas airport (Italy).

Cloud type	Frequency of occurrence (%)	Liquid water column (mm)	1.55-μm cloud attenuation (dB)
Stratus	57.0	0.004	3.5
Nimbostratus	19.5	0.039	23.5
Cumulus	14.8	0.162	95.5
Cumulonimbus	8.6	0.475	280.2

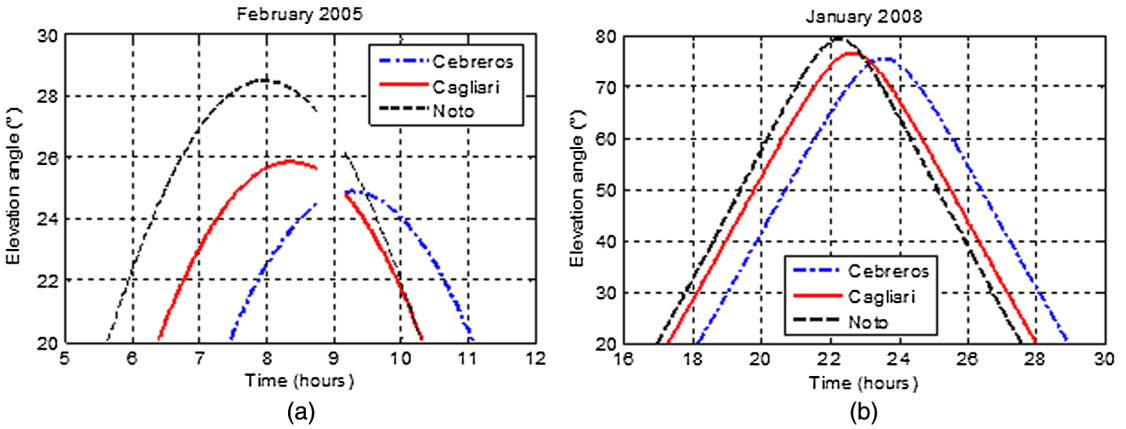

Fig. 2 Shortest (a) and longest (b) visibility windows of Mars Express Orbiter from the selected deep-space (DS) stations.

and December 1987 is associated to December 2012. In addition, each cloud profile derived from a radiosonde measurement collected in a given month of P1 has been considered to possibly occur in any minute of the associated month in P2. This procedure allows both to increase the statistical significance of the results and to exploit as much as possible the information available from RAOBS data. In fact, as long as statistics of optical attenuation are of interest, the key point is to estimate the optical transmissivity through clouds using a complete database of meteorological conditions representative of the local climate, regardless of the exact time they may occur.

Figure 3 depicts the percentage of the visibility time when the optical attenuation A (wavelength = 1.55 μm) induced by clouds (water plus ice) exceeds a given threshold. The curves in Fig. 3, also known as complementary cumulative distribution functions (CCDFs), have been obtained by first calculating A_V as the integration of the vertical profile of the total specific attenuation (i.e., due both to liquid water and ice) as shown in Eq. (5), in turn obtained from each RAOBS ascent. Finally, under the assumption of local horizontal uniformity of clouds,[20] A_V has been scaled as $A = A_V / \sin(\theta)$ using all the values of elevation angle θ in each visibility window of the associated month.

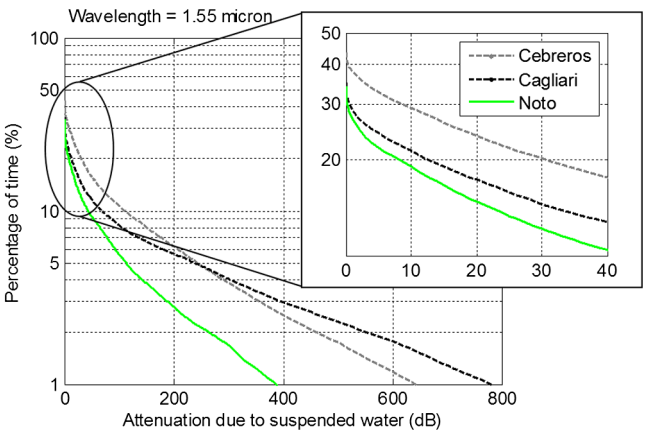

Fig. 3 Percentage of the visibility time when the optical attenuation A induced by clouds (water plus ice) exceeds a given threshold for the three DS stations.

The CCDFs in Fig. 3 indicate that Noto is the best choice for the installation of a DS OCL. The probability of cloud occurrence (i.e., the probability that cloud attenuation is greater than zero) is 34% in Noto, 35% in Cagliari and 44% in Cebreros, respectively. Nevertheless, given the extremely high values of optical attenuation impairing the communication system, no OCL is actually feasible: even in Noto, ~40 dB of link margin would be required to counteract cloud attenuation for 10% of the visibility time.

4 Diversity Schemes

In order to mitigate the extremely high path loss caused by clouds, site diversity schemes may be adopted, for which the lowest path attenuation experienced by all the considered receiving stations, simultaneously connected to the space probe, is selected. The two-site and three-site diversity configurations consisting of the mentioned DS stations is depicted in Fig. 4, which also reports the distance between the sites, ranging between 574 and 1722 km for the closest (Cagliari and Noto) and most remote (Noto and Cebreros) sites.

Using concurrent data in the RAOBS database, the effectiveness of site diversity schemes in mitigating cloud attenuation is quantified in Fig. 5, which depicts the CCDFs of the cloud attenuation for two-station (Cebreros-Noto) and three-station (Cebreros-Noto-Cagliari) diversity systems. These curves have been calculated by always selecting, at each "time," the lowest attenuation value among those simultaneously suffered from the diversity links for which the probe is in visibility. Making reference to Fig. 2, this means that,

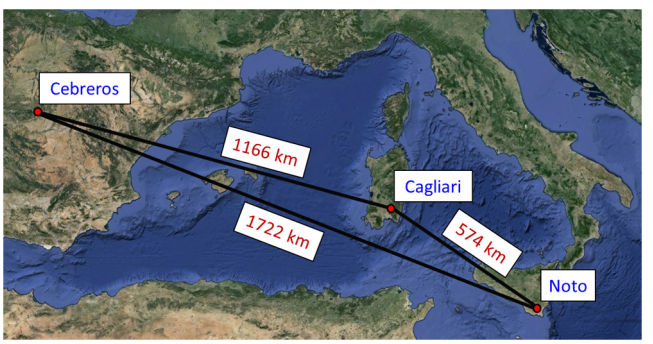

Fig. 4 Sketch of the two- and three-site diversity configurations considered.

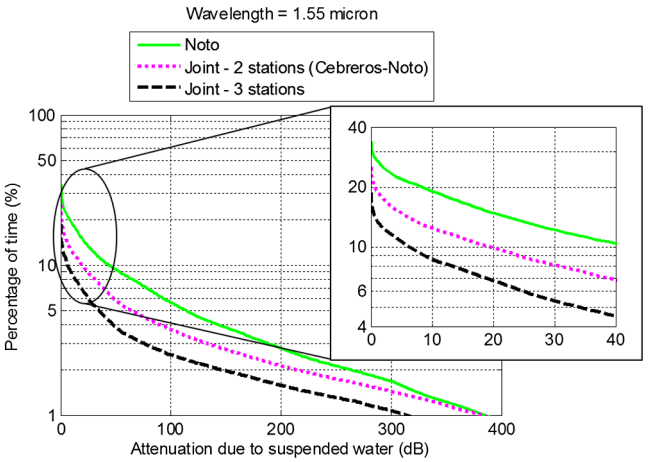

Fig. 5 Complementary cumulative distribution function (CCDF) of the optical attenuation due to clouds for Noto and for the two- and three-site diversity systems. DS scenario.

owing to the different longitude of the selected DS sites, the communication system cannot always take full advantage of the site diversity scheme, as in some time intervals only 1 or 2 links can simultaneously see the probe. On the other hand, the larger the distance D between the sites, the higher the spatial decorrelation of clouds: as D increases, it is less and less likely that heavy clouds simultaneously impair all the links and, consequently, the site diversity gain increases too when the probe is visible by all the stations involved in the scheme. For convenience, Fig. 5 also includes the CCDF of attenuation relative to the station in Noto, thus allowing to better quantify the advantage of implementing site diversity: the link margin to counteract cloud attenuation for a system with target availability of 90% reduces from at least 40 dB for the most suitable site (Noto) to ~20 and 6 dB for the two- and three-site diversity scheme, respectively; on the other hand, considering a link margin of 6 dB, the employment of multiple stations allows the connectivity time to increase from 78% (only Noto) to 86% (two sites) or 90% (three sites).

For the sake of comparison, the same methodology described above has been applied to a different scenario

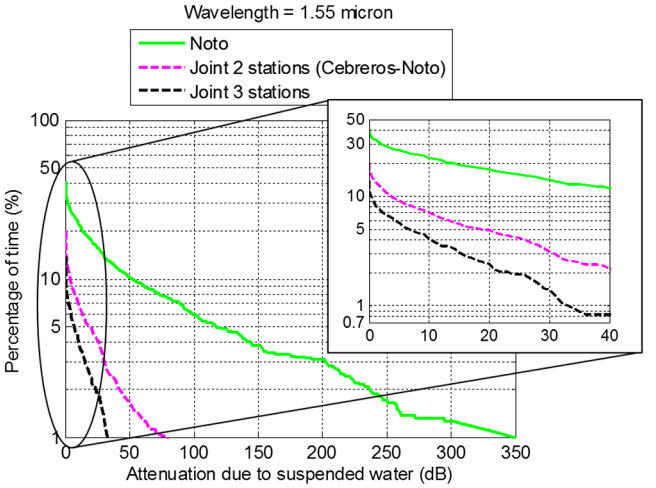

Fig. 6 The CCDF of the optical attenuation due to clouds for Noto and for the two- and three-site diversity systems. Geostationary satellite (orbital position = 5°E) scenario.

involving a geostationary (GEO) satellite with orbital position 5°E. We have considered the same ground stations and the same ROABS dataset for the prediction of cloud attenuation as in the DS case. The results for this scenario are reported in Fig. 6, which, similarly to Fig. 5, depicts the CCDF of cloud attenuation obtained for Noto, as well as for the joint use of two (Cebreros and Noto) or three stations. For the GEO satellite scenario, site diversity appears to be much more effective than in the DS case: the link margin needed to counteract cloud attenuation with target availability of 90% reduces from roughly 50 dB for Noto to ~3.5 and 0.3 dB for the two- and three-site diversity scheme, respectively. These results are prevalently due to (constant) elevation angles in the order of 35 deg /45 deg for the GEO case (specifically, between 42 and 46 deg in this case study), while, on the contrary, the DS scenario involves much lower values of θ (i.e., higher values of cloud attenuation) for quite a large fraction of the visibility time (refer to Fig. 2). Moreover, in the GEO case, it is possible to take full advantage of site diversity because the satellite is always simultaneously visible from the three stations while this is only partially true in the DS scenario.

5 Conclusions

We have investigated the possible use of FSO links in DS missions, specifically focusing on the detrimental effects of clouds. Based on a large dataset of RAOBS, we have quantified the impact of different cloud type on FSO links, showing that the effects of stratus clouds, by far the most common type of cloud, can be counteracted with quite limited link margins (3.5 dB on average). We have predicted the performance of an optical communication system between Earth stations in the Mediterranean area and a DS probe orbiting Mars, showing that, while no sufficient connectivity is attainable using a single station, site diversity schemes can be successfully implemented to considerably reduce the overall link margins for cloud attenuation to acceptable levels: the margin for cloud attenuation for a system with target availability of 90% reduces from 40 dB for one site (Noto) to roughly 20 and 6 dB for the two- and three-site diversity scheme, respectively; on the other hand, with a margin of 6 dB, the connectivity time increases from 78% (only Noto) to 86% (two sites) or 90% (three sites).

Acknowledgments

The authors would like to thank Dr. Antonio Martellucci from the European Space Agency for granting access to the FERAS database.

References

1. C. C. Davis, I. I. Smolyaninov, and S. D. Milner, "Flexible optical wireless links and networks," *IEEE Comm. Mag.* **41**(3), 51–57 (2003).
2. S. Arnon et al., Eds., *Advanced Optical Wireless Communication Systems*, Cambridge University Press, Cambridge, UK (2012).
3. Interagency Operations Advisory Group, "Optical link study group final report," 15 June 2012, https://www.ioag.org/Public%20Documents/Forms/AllItems.aspx (15 June 2012).
4. H. Hemmati, A. Biswas, and I. B. Djordjevic, "Deep-space optical communications: future perspectives and applications," *Proc. IEEE* **99**(11), 2020–2039 (2011).
5. NASA, "Lunar Atmosphere and Dust Environment Explorer (LADEE)," 14 January 2014, http://www.nasa.gov/mission_pages/ladee/main/#.UvSlpLTw9Cg (7 February 2014).
6. M. R. Garcia-Talavera et al., "Ground to space optical communication characterization," *Proc. SPIE* **5892**, 1–16 (2005).

7. A. Biswas and S. Piazzolla, "The Atmospheric Channel," Chap. 3 in *Deep Space Optical Communications*, H. Hemmati, Ed., pp. 121–213, Wiley, New York (2006).
8. A. Biswas and S. Piazzolla, "Deep-space Optical Communications Downlink Budget from Mars: System Parameters," IPN Progress Report 42-154, Jet Propulsion Laboratory, Pasadena, California (2003).
9. E. P. Shettle, "Models of aerosols, clouds and precipitation for atmospheric propagation studies," in *Proc. AGARD Conference No. 454, Atmospheric Propagation in the UV, Visible, IR, and MM-Wave Region and Related Systems Aspects*, Copenhagen, Denmark, pp. 15-1–15-13 (1989).
10. A. W. Dissanayake, J. E. Allnutt, and F. Haidara, "A prediction model that combines rain attenuation and other propagation impairments along Earth-satellite paths," *IEEE Trans. Ant. Prop.*, **45**(10), 1546–1558 (1997).
11. A. Benarroch et al., "Precipitation, clouds and other related non-refractive effects," Chap. 3.2 in *COST Action 255 Final Report—Precipitation, Clouds and Other Related Non-Refractive Effects*, R.A. Harris, Ed., ESA Publication Division, Noordwijk, The Netherlands (2002).
12. E. Salonen and W. Uppala, "New prediction method of cloud attenuation," *Electron. Lett.* **27**(12), 1106–1108 (1991).
13. A. Martellucci, J. P. V. Poiares Baptista, and G. Blarzino, "New climatological databases for ice depolarisation on satellite radio links," in *1st International Workshop of COST 280*, Malvern, UK (2002).
14. Rec. ITU-R P.840-5, *Attenuation due to clouds and fog*, International Telecommunication Union, Geneva (March 2012).
15. L. Luini et al., "Attenuation in non rainy conditions at millimeter wavelengths: assessment of a procedure," *IEEE Trans. Geosci. Remote Sens.* **45**(7), 2150–2157 (2007).
16. C. Capsoni, L. Luini, and R. Nebuloni, "Prediction of cloud attenuation on earth-space optical links," in *6th European Conference on Antennas and Propagation (EuCAP)*, Prague, Czech Republic, pp. 326–329, IEEE, Piscataway, New Jersey (2012).
17. C. M. R. Platt, "A parameterization of the visible extinction coefficient of ice clouds in terms of the ice water content," *J. Atmos. Sci.* **54**(16), 2083–2098 (1997).
18. ESA, "Mars Express overview," 29 May 2013, http://www.esa.int/Our_Activities/Space_Science/Mars_Express_overview (7 February 2014).
19. NASA, "The SPICE toolkit webpage," 11 June 2010, http://naif.jpl.nasa.gov/naif/toolkit.html (7 February 2014).
20. L. Luini and C. Capsoni, "A methodology to generate cloud attenuation fields from NWP products," in *6th European Conference on Antennas and Propagation (EuCAP)*, Prague, Czech Republic, pp. 1482–1486, IEEE, Piscataway, New Jersey (2012).

Lorenzo Luini received his laurea degree in telecommunication engineering in 2004 and his PhD in information technology in 2009, both from Politecnico di Milano, Italy. He is currently an assistant professor at DEIB (Dipartimento di Elettronica, Informazione e Bioingegneria), Politecnico di Milano. Since 2004, his research activities have been relative to electromagnetic wave propagation through the atmosphere, at both radio and optical frequencies.

Roberto Nebuloni received his laurea degree in electronic engineering and his PhD degree in information engineering from the Politecnico di Milano, Milan, Italy, in 1997 and 2004, respectively. He is currently a senior researcher at the Istituto di Elettronica e Ingegneria Informatica e delle Telecomunicazioni (IEIIT) of the Italian National Research Council (CNR), Milan. His research interests include millimeter and optical-wave propagation, satellite systems and radar applications in the fields of telecommunications and meteorology.

Carlo Capsoni graduated in electronic engineering at Politecnico di Milano in 1970. He was a researcher of the Italian National Research Council and then moved to Politecnico, where he became full professor of electromagnetics in 1986. His scientific activity is mainly concerned with theoretical and experimental aspects of electromagnetic wave propagation from centimeter to optical wavelengths in presence of atmospheric degradations, with channel modeling and with design of advanced satellite communication systems.